Non-coding RNA Research 9 (2024) 330–340

Contents lists available at ScienceDirect

Non-coding RNA Research

journal homepage: www.keaipublishing.com/en/journals/non-coding-rna-research

Original Research Article

Exosomal MALAT1 promotes the proliferation of esophageal squamous cell carcinoma through glyoxalase 1-dependent methylglyoxal removal

Liwen Hu [a,1], Kai Xie [a,b,1], Chao Zheng [a,c,1], Bingmei Qiu [a,1], Zhisheng Jiang [a], Chao Luo [a], Yifei Diao [a], Jing Luo [a,***], Xinyue Yao [d,**], Yi Shen [a,*]

[a] Department of Cardiothoracic Surgery, Jinling Hospital, Medical School of Nanjing University, Nanjing, China
[b] Department of Thoracic Surgery, Suzhou Dushu Lake Hospital of Soochow University, Suzhou, China
[c] Department of Thoracic Surgery, National Cancer Center, Chinese Academy of Medical Sciences and Peking Union Medical College, Beijing, China
[d] Department of Laboratory Medicine, Jinling Hospital, Medical School of Nanjing University, Nanjing, China

ARTICLE INFO

Keywords:
Esophageal squamous cell carcinoma
Exosome
MALAT1
Glyoxalase I
KAT2B

ABSTRACT

In previous study we characterized the oncogenic role of long non-coding RNA MALAT1 in esophageal squamous cell carcinoma (ESCC), but the detailed mechanism remains obscure. Here we identified glyoxalase 1 (GLO1) as the most possible executor of MALAT1 by microarray screening. GLO1 is responsible for degradation of cytotoxic methylglyoxal (MGO), which is by-product of tumor glycolysis. Accumulated MGO may lead to glycation of DNA and protein, resulting in elevated advanced glycation end products (AGEs), while glyoxalase 1 detoxify MGO to alleviate its cytotoxic effect to tumor cells. GLO1 interfering led to accumulation of AGEs and following activation of DNA injury biomarkers, which lead to cell cycle arrest and growth inhibition. *In silico* analysis based on online database revealed abundant enrichment of histone acetylation marker H3K27ac in GLO1 promotor, and acetyltransferase inhibitor C646 declined GLO1 expression. Acetyltransferase KAT2B, which was also identified as a target of MALAT, mediated histone lysine acetylation of GLO1 promotor, which was confirmed by ChIP-qPCR experiment. Shared binding sites of miR-206 were found on MALAT1 and KAT2B mRNA. Dual-luciferase reporter assays confirmed interaction within MALAT1-miR-206-GLO1. Finally, we identified MALAT1 encapsuled by exosome from donor cells, and transferred malignant behaviors to recipient cells. The secreted exosomes may enter circulation, and serum MALAT1 level combined with traditional tumor markers showed potential power for ESCC diagnosis.

1. Introduction

Esophageal cancer was ranked as the sixth cause of malignancy-associated mortality [1,2], and esophageal squamous cell cancer (ESCC) was the predominant pathological type in China [3]. The role of long noncoding RNAs (lncRNAs) in ESCC has attracted considerable attention [4]. In addition, in a previous study, we characterized the involvement of lncRNA MALAT1 in ESCC proliferation and metastasis [5], which has been further confirmed by other groups [6–8]. However, there is still a lack of evidence to elucidate the underlying mechanisms.

Using mRNA array screening, we found that glyoxalase I (GLO1) may be the most possible downstream effector of MALAT1. As reported, GLO1 is a ubiquitous enzyme involved in the detoxification of methylglyoxal (MGO) produced during tumor aerobic glycolysis [9], Methylglyoxal is an extremely cytotoxic metabolite that spontaneously glycates proteins and DNA, irreversibly forming toxic compounds called advanced glycation end products (AGEs) [10]. Glycation of DNA contributes to antiproliferative and apoptotic effects, and activates the DNA injury repair pathway to arrest the cell cycle, thus impairing tumor growth. GLO1-mediated degradation is the major method of methylglyoxal detoxification [11], and it antagonizes the adverse effects on tumor growth caused by MGO accumulation, leading to accelerated

* Corresponding author. Department of Cardiothoracic Surgery, Jinling Hospital, Medical School of Nanjing University, 305 East Zhongshan Road, Nanjing, China.
** Corresponding author.
*** Corresponding author. Department of Cardiothoracic Surgery, Jinling Hospital, Medical School of Nanjing University, 305 East Zhongshan Road, Nanjing, China.
E-mail addresses: luojing_2767983@163.com (J. Luo), xinghai0903@163.com (X. Yao), prof_yishen@sina.com (Y. Shen).
[1] The authors contributed equally to this work.

https://doi.org/10.1016/j.ncrna.2024.01.003
Received 18 October 2023; Received in revised form 18 December 2023; Accepted 8 January 2024
Available online 10 January 2024

tumor proliferation.

Being widely accepted as an oncogene, GLO1 in malignant biology has attracted considerable attention [12]. Previous studies have revealed the involvement of GLO1 in gastric [13], breast [14], skin [15], and prostate cancers [16–18], and efforts have been made to develop GLO1-based anticancer therapies [19,20]. To the best of our knowledge, this study is the first to uncover the role of GLO1 in ESCC and to characterize the regulatory mechanism of MALAT1 in enhancing GLO1 expression.

Previous studies have found that excess lncRNAs are encapsulated in exosomes and secreted outside tumor cells, resulting in the transcellular spread of malignant phenotypes [21,22]. Furthermore, tumor cell-derived exosomes may be released into circulation and be used as diagnostic biomarkers [23,24]. In the present study, we verified that intercellular transmission of ESCC-derived exosomes contributes to the spread of the malignant phenotype and explored the potential of serum MALAT1 as a diagnostic biomarker using receiver operating characteristic (ROC) curve analysis.

2. Materials and methods

2.1. Samples and cell lines

The samples used for detection consisted of two independent cohorts. In cohort 1, cancerous and corresponding normal esophageal epithelial tissues were obtained from patients who underwent surgery between July 2016 and June 2019 at the Department of Cardiothoracic Surgery, Jinling Hospital. Patients who received radiotherapy or chemotherapy before surgery were excluded from the study. In cohort 2, whole blood samples were obtained from 98 ESCC patients and 100 healthy controls at Jinling Hospital during the same period for MALAT1 quantification, each of whom donated 10 ml of blood samples. Whole blood samples were centrifuged at 3000×*g* for 10 min to obtain serum samples.

Four esophageal squamous cell carcinoma cell lines (EC109, EC9706, KYSE150, and KYSE450) were obtained from the Cell Bank of the Chinese Academy of Sciences (Shanghai, China) and the Cancer Institute and Hospital, Chinese Academy of Medical Sciences (Beijing, China). The cells were cultured in RPMI-1640 medium (Hyclone, USA) supplemented with 10 % fetal bovine serum (FBS) and maintained in a humidified incubator at 37 °C with 5 % CO_2.

This study was approved by the Research Ethics Committee of the Jinling Hospital. Written informed consent for biological research was obtained from all participants. The study was conducted in accordance with the 1975 Declaration of Helsinki.

2.2. Isolation and identification of exosomes

The serum or cell culture medium (1.5 ml) was centrifuged at 2000×*g* at 4 °C for 30 min, and the supernatant was transferred and further centrifuged at 10,000×*g* at 4 °C for 45 min. The supernatant was then collected and filtered through a 0.22 μm filter (Millipore, USA). The filtrate was collected and subjected to ultracentrifugation at 10,000×*g* and 4 °C for 70 min. The precipitate was resuspended in 10 ml of pre-cooled 1 × PBS and ultracentrifugation was repeated. Finally, the isolated exosomes were resuspended in 1.5 ml of pre-cooled 1 × PBS and characterized using transmission electron microscopy. Exosome concentration-particle size testing (NTA) was performed using ZetaView (Particle Metrix Ltd., Germany).

2.3. RNA extraction and qRT-PCR

Total RNA was isolated from the tissues, serum, and cell cultures using TRIzol reagent (Takara, Japan) according to the manufacturer's instructions. cDNA was synthesized from 200 ng of RNA using the PrimeScript RT reagent Kit (Takara, Japan) and amplified by quantitative real-time PCR with SYBR Green Kit (Takara, Japan) on an Illumina Eco™ (Illumina, USA). GAPDH was used as an internal reference, and the relative expression levels of mRNAs were normalized to GAPDH using $2^{-\triangle\triangle t}$. Primers are listed in Supplementary Table S1.

2.4. RNA interfering and overexpression

The cells were cultured in six-well plates at a density of 3×10^5/well overnight. siRNA or the negative control at a final concentration of 100 nM was separately transfected into cells using Lipofectamine 2000 (Invitrogen, USA) The sequences of the interfering RNA and negative control are provided in Supplementary Table S1 pcDNA3.1, was used for GLO1 overexpression. The interfering or overexpression efficiency was determined by qRT-PCR or western blotting 48 h post-transfection as described [5].

2.5. Expression profile screening

MALAT1 was knocked down using siRNA in EC109 cells for further microarray analysis. Total RNA was extracted as described above, and RNA quality was determined using standard denaturing agarose gel electrophoresis and NanoDrop ND-1000 (Thermo, USA). mRNA microarray screening was performed using GeneChip® Human Transcriptome Array 2.0 (Affymetrix, USA), and miRNA microarray screening was performed using Affymetrix GeneChip miRNA 4.0 Array.

2.6. CCK8 and edu assays

A Cell Counting Kit 8 (Djingo, Japan) was used for cell viability analysis. Cells transfected with siRNAs or a negative control (NC) were seeded in 96-well plates (5×10^3/well). Viable cells were quantified by measuring the absorbance of reduced WST-8 at 450 nm every 24 h, according to the manufacturer's protocol. Cell proliferation was detected using the Cell-Light EdU Apollo 488 In Vitro Kit (Ribobio, Guangzhou, China) 48 h after the indicated treatments.

2.7. Transwell assays

Cell migration and invasion assays were performed using Costar chambers containing transwell inserts with a pore size of 8 μm (Corning Inc., USA). Cells (5×10^4) transfected with siRNAs or NC were seeded in the upper chamber, coated with or without Matrigel (Invitrogen, USA). Serum-free medium was added to the upper chamber, whereas medium mixed with 20 % FBS was maintained in the bottom chamber. Two days post-incubation, cells in the upper chamber were removed, while cells invading the membrane were fixed with methanol and stained with 0.1 % crystal violet. The invading cells were imaged and counted under a microscope in five random fields (Olympus, Japan).

2.8. Flow cytometric analysis

Cells were seeded on six-well plates at a density of 1.5×10^5 cells/well overnight and then transfected with siRNA or NC as previously described. Two days post-transfection, cells were harvested, fixed with 70 % ethanol for 12 h, and stained with propidium iodide (Beyotime, China). Finally, the stained cells were analyzed by FACS FACSCalibur (BD Bioscience, USA) and Modlfit software (Verity Software House, USA). For apoptosis analysis, the harvested cells were stained with FITC-Annexin V and propidium iodide (Beyotime, China), and the binding of Annexin V-FITC and PI to the cells was read using FACS Calibur (BD Bioscience, USA) and analyzed using Modlfit software (Verity Software House, USA).

2.9. Xenografts mouse model and immunohistochemistry staining

Four-week-old female nude BALB/c mice were housed in laminar flow cabinets under specific pathogen-free conditions and were

randomly allocated into two groups (n = 6 per group). EC109 cells were transfected with lentiviral vectors for si-GLO1 or NC separately, and suspended in PBS. Suspended cells (5×10^6) were subcutaneously injected into a single side of each mouse. Tumor size was measured every three days, and tumor volume was calculated using the formula $TV = ½ \times a \times b^2$ (a = length; b = width). At day 28 post-injection, the mice were sacrificed by cervical dislocation under anesthesia, and the tumors were removed and weighed.

The dissected tumors were embedded in paraffin, and immunohistochemistry was performed using rabbit *anti*-β-actin (Abcam ab124964, UK) and rabbit-*anti*-GLO1 (Abcam ab171121, UK). The results were observed and recorded under a microscope. Animal experiments were approved by the Ethics Committees of Jinling Hospital, and the experimental procedures complied with ethical guidelines.

2.10. Western blotting

Cells were lysed using RIPA reagent (Beyotime, China) mixed with protease inhibitor PMSF (Roche, Switzerland) 48 h after siRNA transfection, and the protein extracts were separated by 10 % SDS-polyacrylamide gel electrophoresis (SDS-PAGE) and then transferred to PVDF membranes (Sigma, USA). The membranes were incubated with specific primary antibodies overnight, followed by incubation with horseradish peroxidase (HRP)-conjugated anti-rabbit secondary antibodies (anti-rabbit) for 1 h. Signals were obtained using an enhanced chemiluminescence chromogenic substrate and visualized on an X-ray film (Fujifilm, Tokyo, Japan). GAPDH was used as a control.

2.11. ELISA

GLO1 knockdown cells and negative controls were collected 48 h after oligo-nucleic acid transfection and subjected to sonication. The cell lysates were collected and sent for ELISA quantification using a commercially available AGE assay kit (MLBio, Shanghai, China), according to the manufacturer's instructions. The AGE concentration-OD450 regression model was acquired by testing the OD450 value of standard samples with different concentrations, and the actual AGE content in each cell line was further calculated based on the resultant regression model.

2.12. Pharmaceutical treatment of ESCC cells

The commercial histone acetyltransferase inhibitor, C646, was used for histone deacetylation (Medchem Express, USA). Cells were seeded in six-well plates (3×10^5/well) overnight and treated with C646 at a final concentration of 20 μM. Twenty-four hours later, the cells were collected and western blotting was performed to test GLO1 protein levels. For the cytotoxicity assay of methylglyoxal, cells were treated with methylglyoxal (0.025 mM) (Sigma Aldrich, USA) for 72 h, and dimethyl sulfoxide (DMSO)-treated cells were used as controls.

2.13. ChIP-qPCR

For chromatin immunoprecipitation (ChIP)-qPCR experiments, cells were seeded in six-well plates (3×10^5 cells/well) and transfected with siRNAs or negative control oligo-nucleic acids. One day post-transfection, the proteins were cross-linked to DNA using 1 % formaldehyde for 15 min. The harvested cells were washed with 1 × PBS and treated with lysis buffer, and the lysates were subjected to ultrasonic vibration to fragment chromatin. Thereafter, 20 μg of cross-linked fragmented chromatin was immunoprecipitated using a commercial EZ-Magna ChIPTM G kit (Millipore, Billerica, MA, USA). Anti-histone H3K27ac (Abcam ab4729, UK) was used, and goat anti-rabbit IgG was used as the negative control. The retrieved DNA was quantified using real-time qPCR analysis. Three target regions of the GLO1 promoter were quantified using the specific primers listed in Supplementary Table S1. The results were calculated as a percentage of the input DNA using the following formula: percentage input = 2 % × 2 (C[T] 2 % input sample − C[T] IP sample).

2.14. Dual-luciferase reporter experiment

Wild-type (wt) or mutant (mut) versions of MALAT1 and GLO1 were synthesized *de novo* and cloned into a Pezx-FR02 vector using digestion and ligation enzymes. The reorganized vectors were named Pezx-FR02-WT and Pezx-FR02-MUT. The reorganized plasmids were verified by DNA sequencing and then co-transfected with miR-206 mimic or miR-NC into HEK293T cells using Lipofectamine™ 2000. Two days post-transfection, cells were lysed and centrifuged for 3–5 min. The Luc-Pair™ Duo-Luciferase HS Assay Kit (GeneCopoeia, Rockville, MD, USA) was used to determine luciferase activity, and internal luciferase activity was used as a reference.

2.15. Exosome labeling and tracing

EC109-derived exosomes were incubated with DiO dye (Rengen Biosciences, China) at 37 °C for 30 min and then added to the culture media of recipient KYSE150 and TE-1 cells. The mixture was incubated at 37 °C, and the cells were stained with DAPI 12 h later (Boster Biological Technology Co., Ltd., China). The cells were observed and imaged using a confocal microscope (Leica, Germany).

2.16. Statistical analysis

Results are presented as the mean ± standard deviation for independent experiments performed in triplicate. Statistical data analysis was performed using R software version 3.6.3. Student's t-test, chi-square test, or one-way ANOVA were used to assess statistical significance, as appropriate. Kaplan–Meier analysis and log-rank tests were used for survival analysis. Receiver operating characteristic (ROC) curves were used to assess the diagnostic performance of the selected biomarkers. A value of $P < 0.05$ was considered statistically significant.

3. Results

3.1. GLO1 acts as a downstream effector of MALAT1

A total of 315 upregulated and 216 downregulated mRNAs were identified as differentially expressed between the negative control (NC) and MALAT1 knockdown (si-MALAT1) EC109 cells (fold change >1.5, $P < 0.05$) (Fig. 1A and B). KEGG pathway analysis suggested that MALAT1 participates in most carcinogenesis-related pathways, including metabolism, extracellular matrix (ECM)-receptor interaction, and PI3K-AKT pathways (Fig. 1C and D). Screening results suggested that GLO1 was the most downregulated gene upon MALAT1 knockdown (Fig. 1A). Data based on GEPIA 2.0 (http://gepia2.cancer-pku.cn/#index) suggested a positive correlation between MALAT1 and GLO1 (Fig. 1E), while data from our previous gene expression analysis also found a positive association between MALAT1 and GLO1 (Fig. 1F, GEO No.: GSE89102). Furthermore, our qRT-PCR results based on 40 ESCC tissues also suggested a roughly linear association (Fig. 1G). We then verified the decreased expression of GLO1 in MALAT1 knockdown ESCC cell lines by qRT-PCR and western blotting (Fig. 1H–J).

3.2. Roles of GLO1 in ESCC malignant phenotypes and MGO detoxification

Data mining showed that GLO1 was significantly elevated in ESCC tissues compared with normal tissues in unpaired tissues (Figs. S1A–B), and gradually increased with lymph node metastasis and TNM stage (Figs. S1C–D). Kaplan–Meier analysis of The Cancer Genome Atlas (TCGA) data demonstrated that patients with higher GLO1 expression

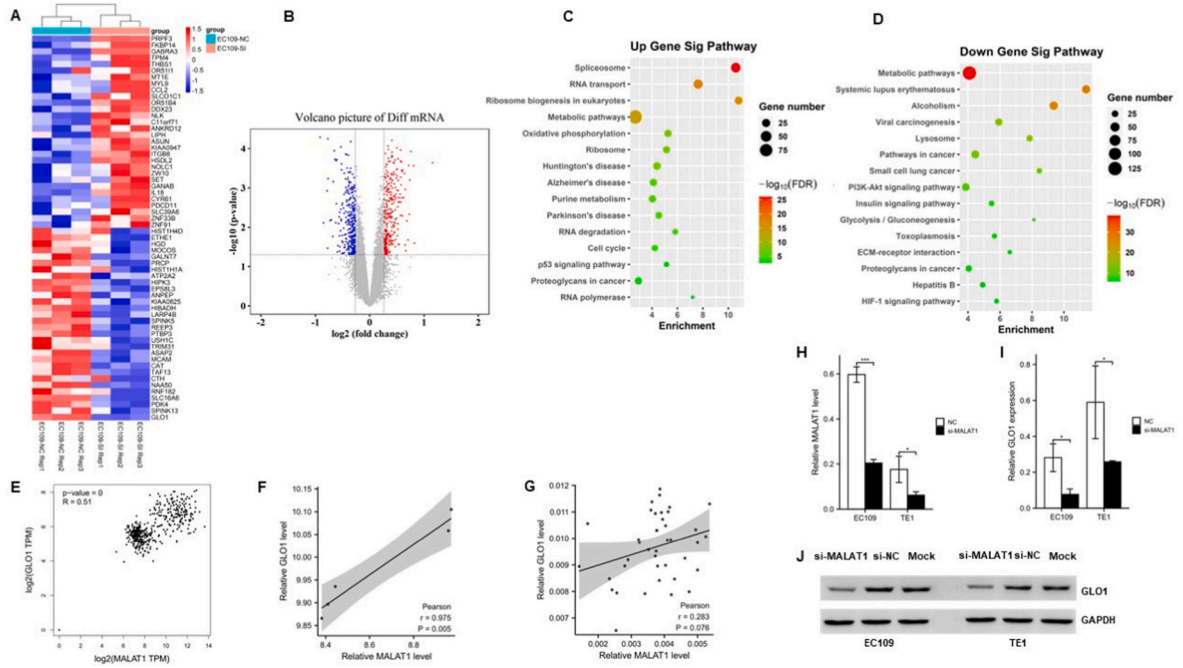

Fig. 1. Microarray screening and validation of MALAT1 downstream target GLO1
A: Hierarchical clustering of MALAT1 target mRNAs derived from three biological replicates. B: Volcano plots analysis of differentially expressed mRNAs upon MALAT1 interfering. C–D: KEGG pathway enrichment analysis of the top up- and down-regulated genes upon MALAT1 knockdown. E: Co-linear association between MALAT1 and GLO1 levels revealed by normalized expression data from TCGA (ESCA tumor) and GTEx (esophagus mucosa) databases. F: Co-expression pattern between MALAT1 and GLO1 derived from GSE89102. G: Person correlation analysis between MALAT1 and GLO1 from forty ESCC tissues. H: Interfering efficacy of MALAT1 by siRNA was detected by qRT-PCR. I: GLO1 mRNA level decreased upon MALAT1 knockdown revealed by qRT-PCR. J: western blotting results suggest decreased GLO1 protein levels induced by MALAT1 knockdown.Data are presented as mean ± SD of triplicate experiments (*p < 0.05, **p < 0.01, ***p < 0.001).

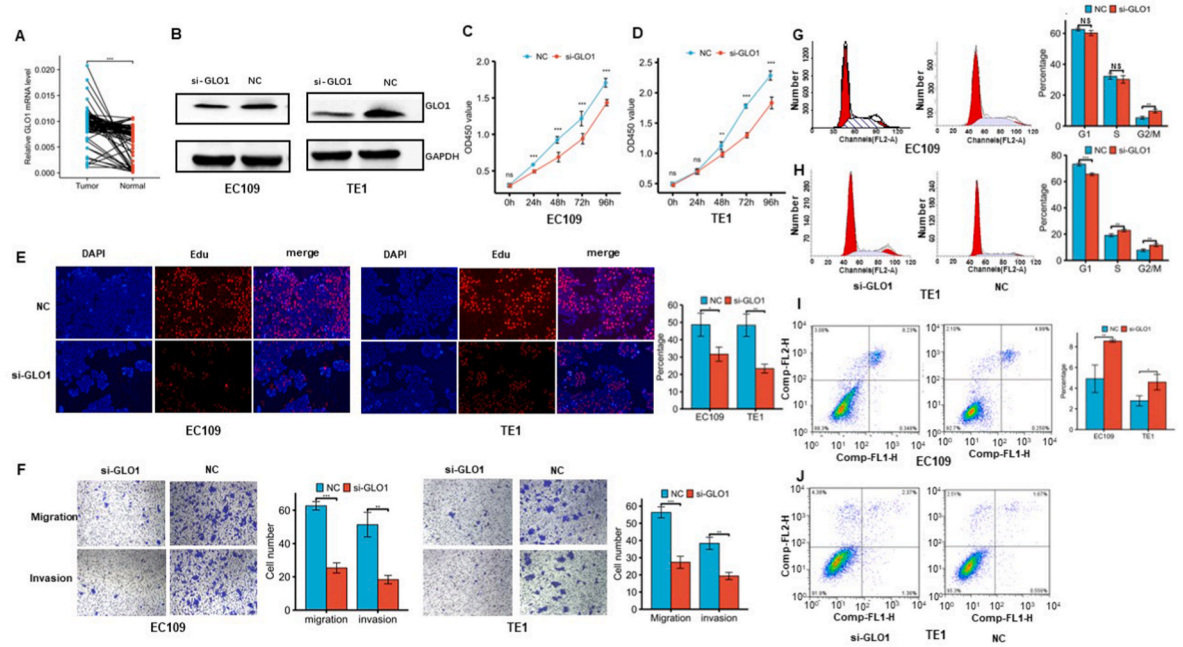

Fig. 2. GLO1 promotes ESCC malignant phenotypes *in vitro*
A: RT-qPCR analysis of GLO1 mRNA levels in 70 paired ESCC and normal esophageal epithelial tissue samples. B: GLO1 protein levels in cells transfected with siRNA or negative control. C–D: Knockdown of GLO1 hampered ESCC cells growth. E: EdU assays performed on cells with GLO1 interfering or negative control. Original magnification, × 200. F: Effects of GLO1 knockdown on the migration and invasion abilities of ESCC cells. The number of cells that migrated or invaded was counted in three different fields. Original magnification, × 200. G–H: Effects of GLO1 knockdown on the cell cycle as assessed by flow cytometry. I–J: Apoptosis analysis of cells with GLO1 interference and negative control, detected by flow cytometric analysis of Annexin-V-FITC/PI staining. Results are presented as the mean ± SD for three biological replicates. Student's t-test was used to analyze the data. *P < 0.05; **P < 0.01; ***P < 0.001.

predicted worse overall, disease-free, and progression-free survival (OS, DFS, and PFS, respectively; Figs. S1E–G). A paired comparison based on TCGA data also suggested GLO1 overexpression in ESCC tissues (Fig. S1H). Our qRT-PCR results from 70 pairs of tumor and corresponding normal tissues further confirmed the overexpression of GLO1 in ESCC tissues (Fig. 2A), and high levels of GLO1 correlated with deep invasion, lymph node metastasis, and advanced stage of ESCC (Supplementary Table S2). We also found GLO1 overexpression in the majority of pan-cancers, indicating that its oncogenic role was prevalent (Fig. S1I).

Knockdown of GLO1 by siRNA (Fig. 2B) dramatically suppressed ESCC cell growth (Fig. 2C and D), proliferation (Fig. 2E), migration, and invasion (Fig. 2F). GLO1 inhibition led to cell cycle arrest at the G2/M phase and increased apoptosis (Fig. 2G–J). Additionally, a xenogeneic mouse model verified the effects of GLO1 (Fig. 3A–F). The rescue experiment showed that ectopic GLO1 expression might reverse the growth inhibition induced by MALAT interference (Fig. 3G–J), supporting the hypothesis that GLO1 acts as a downstream effector.

We next sought to determine AGEs levels and DNA-injury biomarkers 24 h after GLO1 knockdown. The viability of ESCC cells was positively correlated with the concentration of AGEs (Fig. 4A), and MGO significantly inhibited ESCC cell proliferation (Fig. 4B and C). As expected, GLO1 inhibition led to increased levels of AGEs (Fig. 4D and E), coupled with the activation of DNA injury biomarkers (Fig. 4F). Moreover, MALAT1 knockdown activated DNA injury-associated biomarkers and ectopic expression of GLO1 reversed these effects (Fig. 4F), further supporting GLO1 as a downstream effector of MALAT1. MGO treatment of ESCC cells led to the activation of DNA injury biomarkers, which were reversed by GLO1 ectopic expression (Fig. 4G). Furthermore, we found that MGO treatment led to a smaller cell morphology and decreased cell proliferation, which could be reversed by ectopic expression of GLO1 (Fig. 4H and I).

3.3. KAT2B-mediated histone acetylation activates GLO1 expression

Analysis of epigenetic modification biomarkers using the UCSC genome browser (http://genome.ucsc.edu/) revealed abundant enrichment of histone H3K27ac signals around the GLO1 promoter (Fig. 5A). Next, we conducted pharmacological inhibition in ESCC cell lines using the acetyltransferase inhibitor C646, and GLO1 expression was significantly attenuated (Fig. 5B). By re-analyzing the mRNA microarray results, we identified the acetyltransferase KAT2B as a direct target of MALAT1. Downregulation of KAT2B by siRNA abrogated GLO1 protein levels (Fig. 5C and D), and the expression of KAT2B and GLO1 was positively correlated in ESCC tissues (Fig. 5E), indicating the regulatory role of KAT2B in GLO1 expression. We then detected H3K27ac enrichment in the GLO1 promoter using CHIP-qPCR, and the results indicated that H3K27ac was weaker upon KAT2B downregulation (Fig. 5F–I).

3.4. MALAT1 regulates KAT2B expression through a competing endogenous RNA (ceRNA) mechanism via miR-206

First, we verified that knockdown of MALAT1 suppressed KAT2B expression by western blotting (Fig. 6A), and data from the GEPIA 2.0 database suggested that MALAT1 positively correlated with KAT2B in ESCC ($R = 0.17$, $P = 0.022$; Fig. 6B). We started with profile screening of miRNA targets for MALAT1 using three independent sets of microarrays (Fig. 6C), followed by prediction of lncRNA-miRNA-mRNA interaction on ENCORI (https://starbase.sysu.edu.cn/, Figs. S2A–C). Microarray analysis revealed that miR-206 is a MALAT1 target, while MALAT1 and KAT2B shared common binding sites of miR-206 (Fig. 6D), and MALAT1 knockdown resulted in elevated miR-206 levels (Fig. 6E). Ectopic expression of miR-206 using mimics suppressed MALAT1 and KAT2B expression (Fig. 6F–H), and we confirmed the degradation effects of miR-206 on MALAT1 and KAT2B using a luciferase reporter system (Fig. 6I and J). Furthermore, ectopic expression of miR-206 reversed the

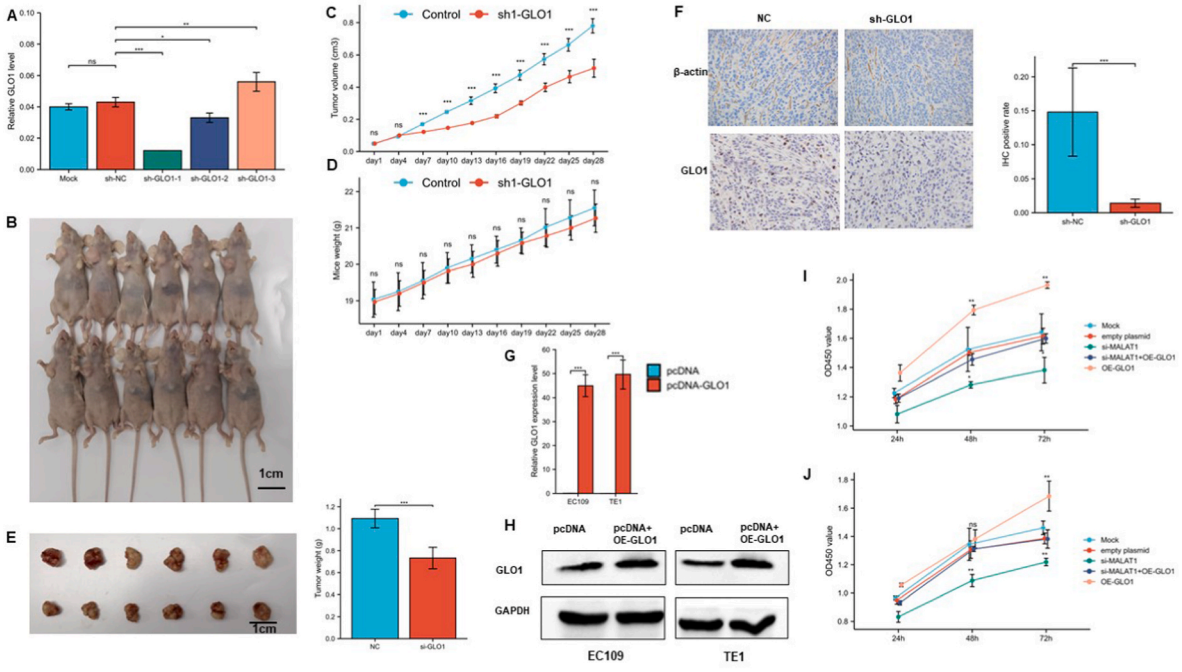

Fig. 3. GLO1 promotes ESCC tumor formation *in vivo* and rescues cell growth inhibition induced by MALAT1 interfering. A: Interfering efficiency of sh-GLO1 lentivirus. B: Images of mice from different treatment groups four weeks after tumor injection. C–D: Quantification of tumor volume and mouse weight in subjects injected with EC109 cells transfected with sh-NC or sh-GLO1 lentivirus vector during the four weeks period. E: The dissected tumors were photographed (left), and tumor weight decreased in the GLO1 knockdown mice group (right). F: Representative images for immunohistochemical staining of GLO1 in tumor nodes dissected from different groups (left). IHC score of GLO1 staining in sh-GLO1 and sh-NC samples (right). G–H: Analysis of ectopic expression of GLO1 in EC109 and TE1 cells at the mRNA (G) and protein (H) levels. I–J: Ectopic expression of GLO1 promoted tumor growth and restored the inhibitory effect of si-MALAT1 in EC109 and TE1 cellsData are presented as the mean ± SD of triplicate experiments; *P < 0.05; **P < 0.01; ***P < 0.001; ns not significant.

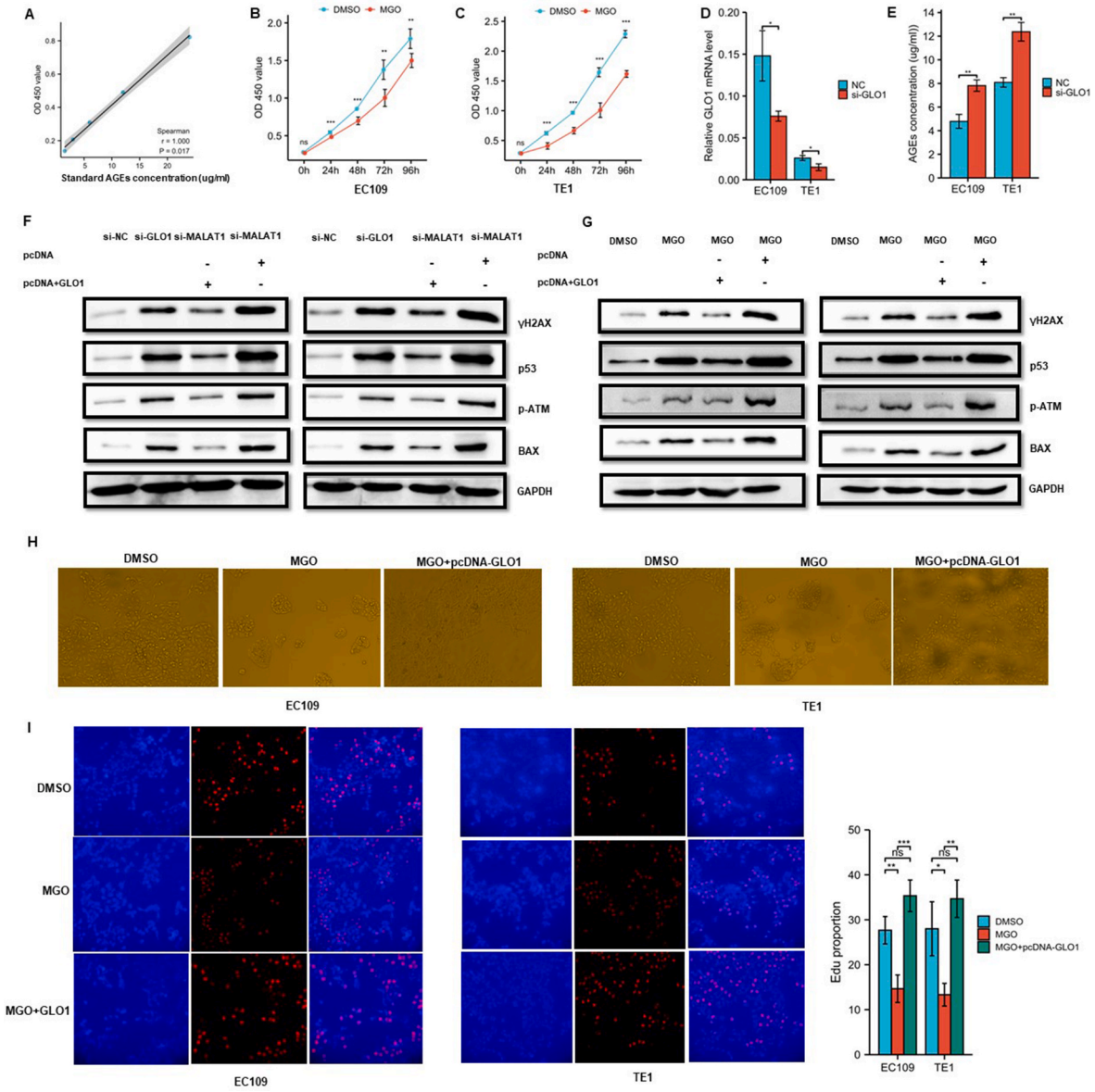

Fig. 4. GLO1 knockdown led to cytotoxic effects and DNA injury marker activation
A: Standard AGEs-OD450 value correlation curve. B-C: Effects of exogenous methylglyoxal on ESCC growth were determined by CCK8 analysis. D: Interfering efficacy of GLO1 by siRNA. E: ELISA analysis showed that GLO1 knockdown resulted in elevated AGEs concentration in the culture medium. F: MALAT1 knockdown activated DNA injury-associated biomarkers, and ectopic expression of GLO1 reversed the effects induced by MALAT1 knockdown. G: DNA injury biomarkers are activated by MGO treatment and reversed by ectopic GLO1 expression. H: MGO treatment led to cell shrinkage in morphology, as detected by cell microscopy, whereas ectopic expression of GLO1 reversed these effects. I: The MGO treatment-induced decrease in cell proliferation was reversed by ectopic expression of GLO1. *P < 0.05; **P < 0.01; ***P < 0.001; ns not significant.

inhibitory effect of KAT2B on MALAT1 knockdown (Fig. 6K). qRT-PCR results from ESCC tissues indicated an obvious positive correlation for MALAT1 and KAT2B (Fig. 6L), as well as an inverse correlation for MALAT1-miR-206 and KAT2B-miR-206 (Fig. 6M – N). Using data mining, we found that miR-206 expression was relatively lower in ESCC tissues (Fig. S3A), especially in advanced stages (Figs. S3B–C), and ectopic expression of miR-206 by mimics inhibited ESCC growth (Figs. S3D–E), migration, and invasion (Figs. S3F–G). These findings suggest that miR-206 acts as a tumor suppressor in ESCC, which is supported by its antagonistic role in MALAT1.

3.5. Transcellular spread of malignant phenotypes induced by exosomal MALAT1 and liquid detection based on serum MALAT1

We separated exosomes from the culture medium of ESCC cell lines and quantified MALAT1 expression in the exosomes. Electron microscopy and concentration-particle size testing confirmed the morphological patterns (Fig. 7A and B). The qRT-PCR results showed expression levels among the four ESCC cell lines (Fig. 7C). These findings showed that exosomal MALAT1 from EC109 surpasses all others. We then isolated exosomes from EC109 cells and co-cultured them with KYSE150 and TE-1 cells (Fig. 7D). Twenty-four hours later, we detected upregulated MALAT1 levels in recipient cells (Fig. 7E), which exhibited accelerated growth (Fig. 7F and G). To evaluate the clinical significance of exosomal MALAT1, we measured serum exosomal MALAT1 levels in 98 ESCC serum samples and 100 healthy donors (Fig. 7H). The distribution of demographic characteristics for the cases and controls is listed in Supplementary Table S3. Serum MALAT1 was elevated in an orderly manner according to the tumor grade. High exosomal MALAT1 levels were mostly found in middle- and late-stage ESCC patients but not in

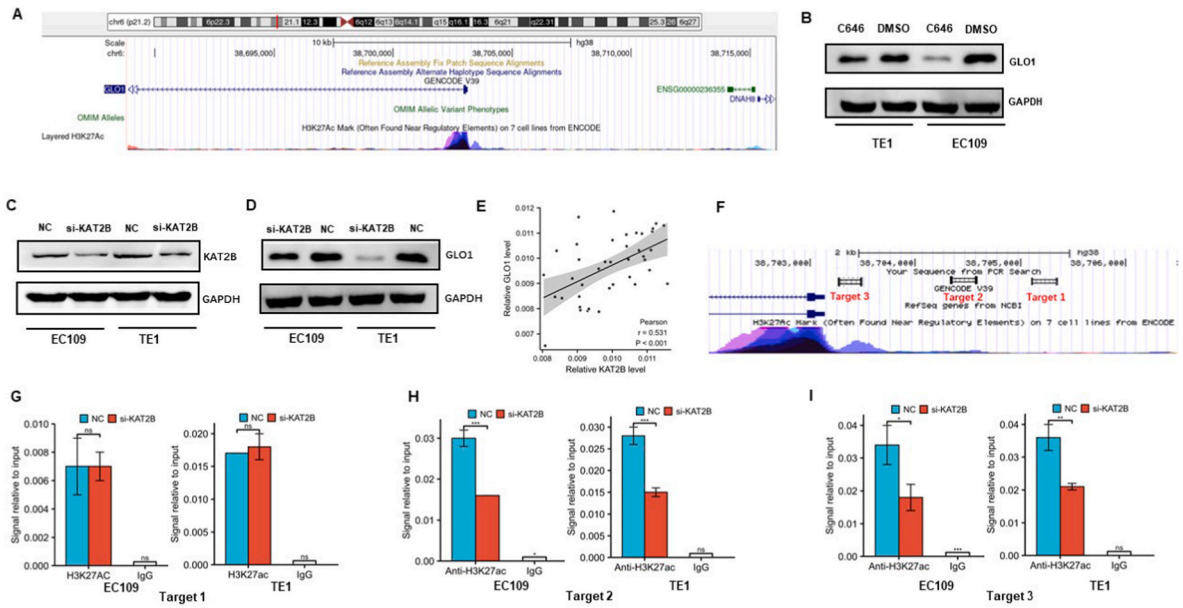

Fig. 5. GLO1 expression was regulated by histone H3K27ac modification on its promotor
A: Screenshot of the UCSC genome browser view showing genomic features of the GLO1 promoter. B: Histone acetyltransferase inhibitor C646 suppressed GLO1 protein expression. C: Efficiency of knockdown for acetyltransferase KAT2B by siRNA. D: Knockdown of acetyltransferase KAT2B led to the repression of GLO1 expression according to western blotting analysis. E: Pearson correlation analysis between KAT2B and GLO1 in forty ESCC tissues. F: Schematic illustration of indicated targets for qPCR following CHIP assays. G–I: ChIP-qPCR revealed that KAT2B knockdown decreased H3K27ac acetylation at the promoter region of GLO1 at two separate locations. *P < 0.05; **P < 0.01; ***P < 0.001; ns not significant.

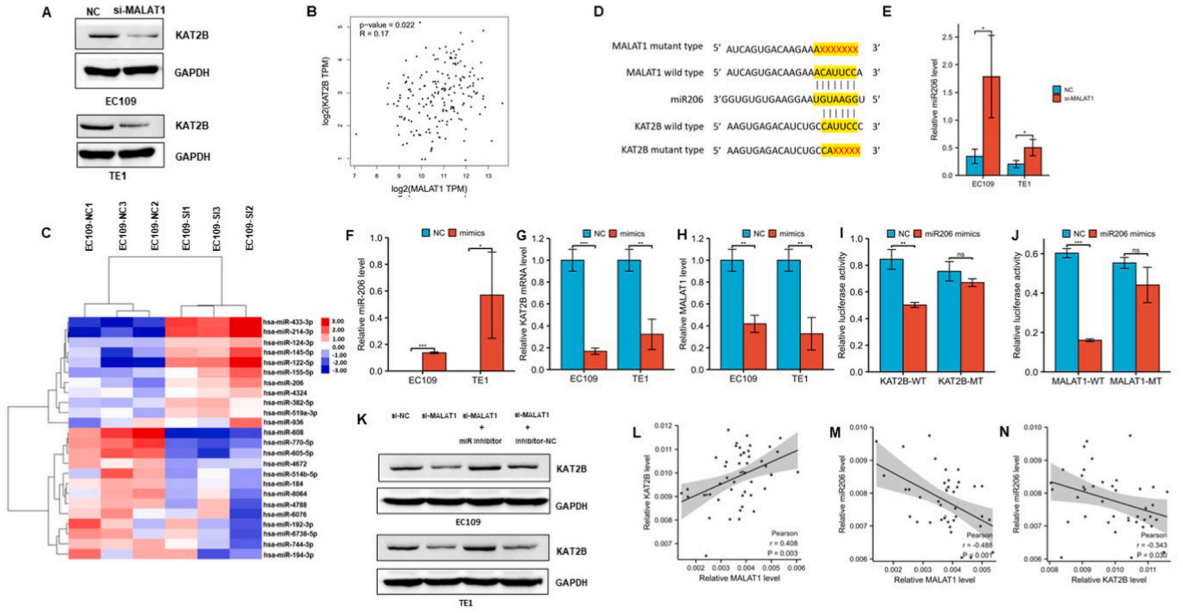

Fig. 6. MALAT1 regulates KAT2B expression through ceRNA mechanism
A: Western-blotting results confirmed knockdown of MALAT1 decreased KAT2B protein level. B: Co-expression between MALAT1 and GLO1 mRNA revealed by TCGA database and analysis performed using GEPIA. C: Heatmap for microarray analysis of MALAT1 target miRNAs. D: Sequences of reporter constructs containing the wild-type or mutant binding site (BS) of miR-206. E: qRT-PCR confirmation of miR-206 in MALAT1 knockdown cells. U6 was used as an internal control for miRNA quantification. F: The efficiency of ectopic expression of miR-206 by mimics. G–H: Effects of miR-206 mimics on KAT2B and MALAT1 RNA level. I–J: Luciferase reporter activity of wild-type (WT) or mutated (MUT) reporter in 293T cells co-transfected with miR-206 mimics or NC. K: Ectopic expression of miR-206 rescued the inhibition of the KAT2B protein induced by MALAT1 knockdown. L–N: Pearson correlation analysis for MALAT1-KAT2B, MALAT1-miR206, and KAT2B-miR206 pairs in the same set of 40 ESCC tissues.*P < 0.05, **P < 0.01, ***P < 0.001, n.s, no significance.

healthy and early stage patients (Fig. 7I). Furthermore, we found no significant difference between serum total MALAT1 and serum exosomal MALAT1 levels, suggesting that serum MALAT1 exists mainly in exosomes (Fig. 7J). A diagnostic model based on serum MALAT1 achieved moderate performance in ESCC diagnosis, with an area under the curve (AUC) value of 0.755 (CI = 0.686–0.824), which is superior to that of the classic tumor marker (Fig. 7K). Combined ROC analysis integrating MALAT1 and the three biomarkers improved diagnostic performance, with an AUC value of 0.834 (CI = 0.775–0.893; Fig. 7L).

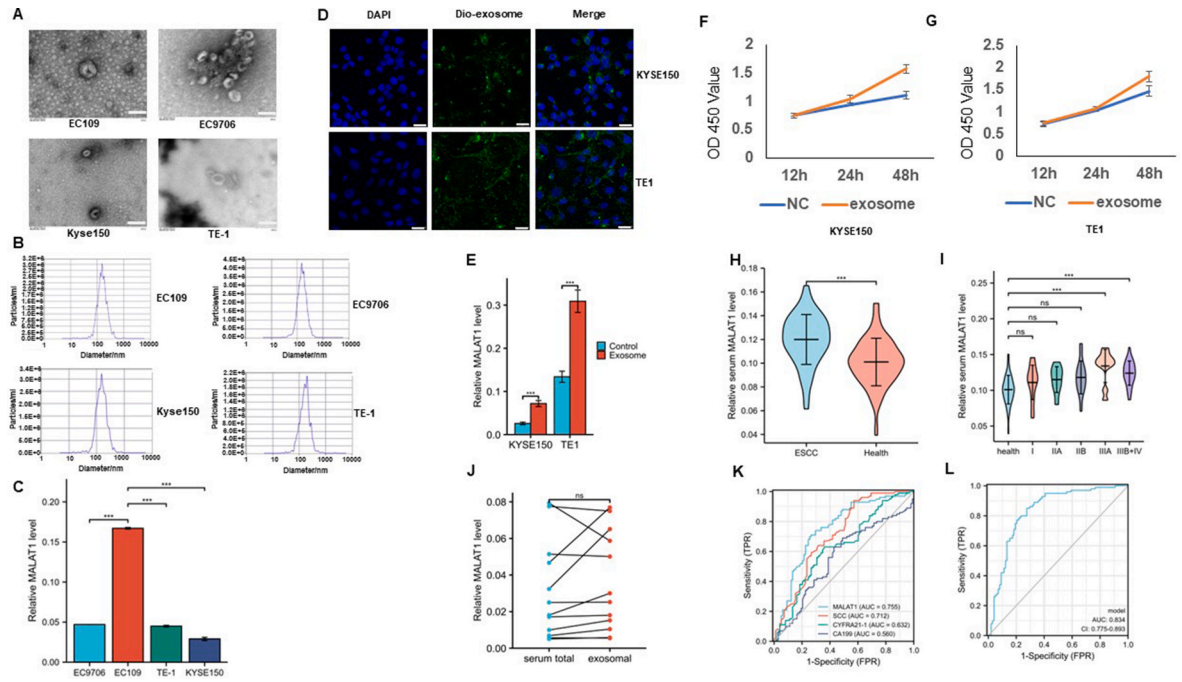

Fig. 7. Exosomal MALAT1 mediated intercellular transmission of malignant phenotype and its application in ESCC non-invasive diagnosis. A: Identification of exosomes from different ESCC cell lines by transmission electron microscope. Scale bar = 200 nm. B: Concentration-particle size testing of isolated exosomes. C: The levels of exosomal MALAT1 in the four ESCC cell lines determined by quantitative RT-qPCR. D: Representative confocal images showing the delivery of Dio-labeled exosomes (EC109-derived) to DAPI-labeled KYSE150 and TE1 cells. Scale bar = 25 μm. E: Uptake of EC109-derived exosomes elevates MALAT1 levels in recipient cells by quantitative RT-PCR. F–G: Treatment of EC109-derived exosomes enhanced recipient cells growth capability; H: Unpaired comparison of serum MALAT1 level between ESCC patients and healthy controls. I: Serum MALAT1 level ascended as ESCC stages. J: No significant difference was found between serum total and exosomal MALAT1 level. K: ROC analysis for serum MALAT1 and classic tumor biomarkers in ESCC diagnosis L: Combined ROC analysis integrating MALAT1 and three biomarkers in ESCC diagnosis.*P < 0.05; **P < 0.01; ***P < 0.00.

4. Discussion

In a previous study, we demonstrated the oncogenic role of MALAT1 in ESCC, revealing an association between MALAT1 knockdown and DNA injury repair pathway activation. This association is considered to correlate with cell cycle arrest and growth inhibition [25]. Another study has also provided evidence supporting the depletion of MALAT1-induced DNA damage [26], we wondered how MALAT1 participating in the DNA injury repair pathway was able to promote ESCC growth.

The microarray screening results suggested that GLO1 is a possible target of MALAT1. GLO1 is a member of the glyoxalase system that participates mainly in the degradation of cytotoxic MGO, which is a by-product of tumor glycolysis. MGO binds to proteins and DNAs, leading to glycation of products (AGEs). AGEs can directly produce deleterious effects or exert their damaging effects through the receptors of AGEs (RAGEs). Both MGO and AGEs can induce the most deleterious consequences directly or by stimulating RAGE signaling [27,28].

As the rate-limiting enzyme, glyoxalase 1 catalyzes the conversion of methylglyoxal to S-D-lactyl glutathione in a glutathione (GSH)-dependent manner, followed by the hydrolysis of S-D-lactyl glutathione to non-toxic D-lactic acid performed by glyoxalase 2 [11]. The product S-D-lactyl glutathione promotes microtubule assembly during cell division and is thought to facilitate cell proliferation [11].

MGO metabolism depends mainly on the expression of GLO1 [29,30]. Approximately 2 % of the population had an increased copy number of GLO1. These extra copies can increase the expression of GLO1 and the activity of the enzyme by 2–4 fold [31].

Previous studies have shown that GLO1 expression is regulated at transcriptional [32,33] and post-translational levels [34]. Here, we present the previously unappreciated importance of epigenetic modulation of GLO1 expression. Studies have shown that KAT2B catalyzes histone acetylation modifications of PLK4 [35], TBX5 [36], and CXCL12 [37]. We found that KAT2B knockdown led to weaker H3K27ac deposits and decreased GLO1 expression, confirming that epigenetic modifications of GLO1 contribute to its expression.

Using miRNA array screening and bioinformatics prediction, we identified miR-206 as a mediator of MALAT1 and KAT2B. miR-206 is widely recognized as a tumor suppressor [38–41], and analysis based on a public database also supports its suppressor role in ESCC. The interplay between MALAT1 and miR-206 has been reported in previous studies [42,43], further supporting the ceRNA mechanism for the MALAT1-miR-206-KAT2B axis.

Exosomes are small vesicles secreted by different cell types and covered by a lipid bilayer, with sizes ranging from 50 to 150 nm. Exosomes act in the pathological and physiological environments of target cells by the transcellular transport of different molecules, such as proteins, RNA, and DNA. Previous studies have shown that exosomes from tumor tissues may be released into circulation, and exosomal lncRNAs could be used as liquid biopsy biomarkers. These findings show a promising future for using exosomes for cancer non-invasive screening, especially for gastrointestinal cancers that rely on gastroscopic biopsy. Here, we developed a serum diagnostic model based on serum MALAT1 and traditional tumor biomarkers that could distinguish patients with ESCC from others, suggesting the potential value of serum MALAT1 in ESCC monitoring and follow-up. Our results showed that serum MALAT1 mainly exists in exosomes, which is consistent with a previous study [44], indicating a protective effect of exosomes on lncRNAs, making clinical application possible.

Thus, based on existing data, we concluded that MALAT1 upregulated acetyltransferase KAT2B expression through a competing endogenous RNA (ceRNA) mechanism, and KAT2B further altered the histone H3K27ac abundance on the GLO1 promoter in an epigenetic manner. High GLO1 expression facilitates the degradation of deleterious MGO

produced during glycolysis and reduces the concentration of AGEs, alleviating toxic effects on cell growth (Fig. 8).

Our study has some limitations, such as the limited sample size, which requires multicenter participation and many more samples to confirm the clinical value of serum MALAT1 for ESCC diagnosis and monitoring. Given the advantages of targeting and biological compatibility, recent studies have attempted to reconstruct tumor-derived exosomes as drug cargos, such as siRNAs and chemotherapy drugs [45], which have shown promising prospects. Whether exosomes may be ideal pharmaceutical vectors for MALAT1 or GLO1 target therapy requires further evaluation. Furthermore, the upstream regulator of MALAT1 remains unclear, and we are investigating this in our future work.

5. Conclusions

MALAT1 regulates the expression of KAT2B through a competitive endogenous RNA (ceRNA) way, and changes the histone acetylation of the GLO1 promoter in a KAT2B dependent manner. High GLO1 expression alleviated the toxic effect of methylglyoxal on ESCC cells by facilitating methylglyoxal degradation. ESCC exosome-derived MALAT1 mediates the transfer of oncogenic behavior, and exosomal MALAT1 in the serum may be used as a diagnostic indicator for late-stage ESCC.

Ethics approval and consent to participate

This study was approved by the Research Ethics Committee of the Jinling Hospital. Written informed consent for biological research was obtained from all participants. The study was conducted in accordance with the 1975 Declaration of Helsinki.

Consent for publication

Not applicable.

Availability of data and materials

Additional related data are available upon request.

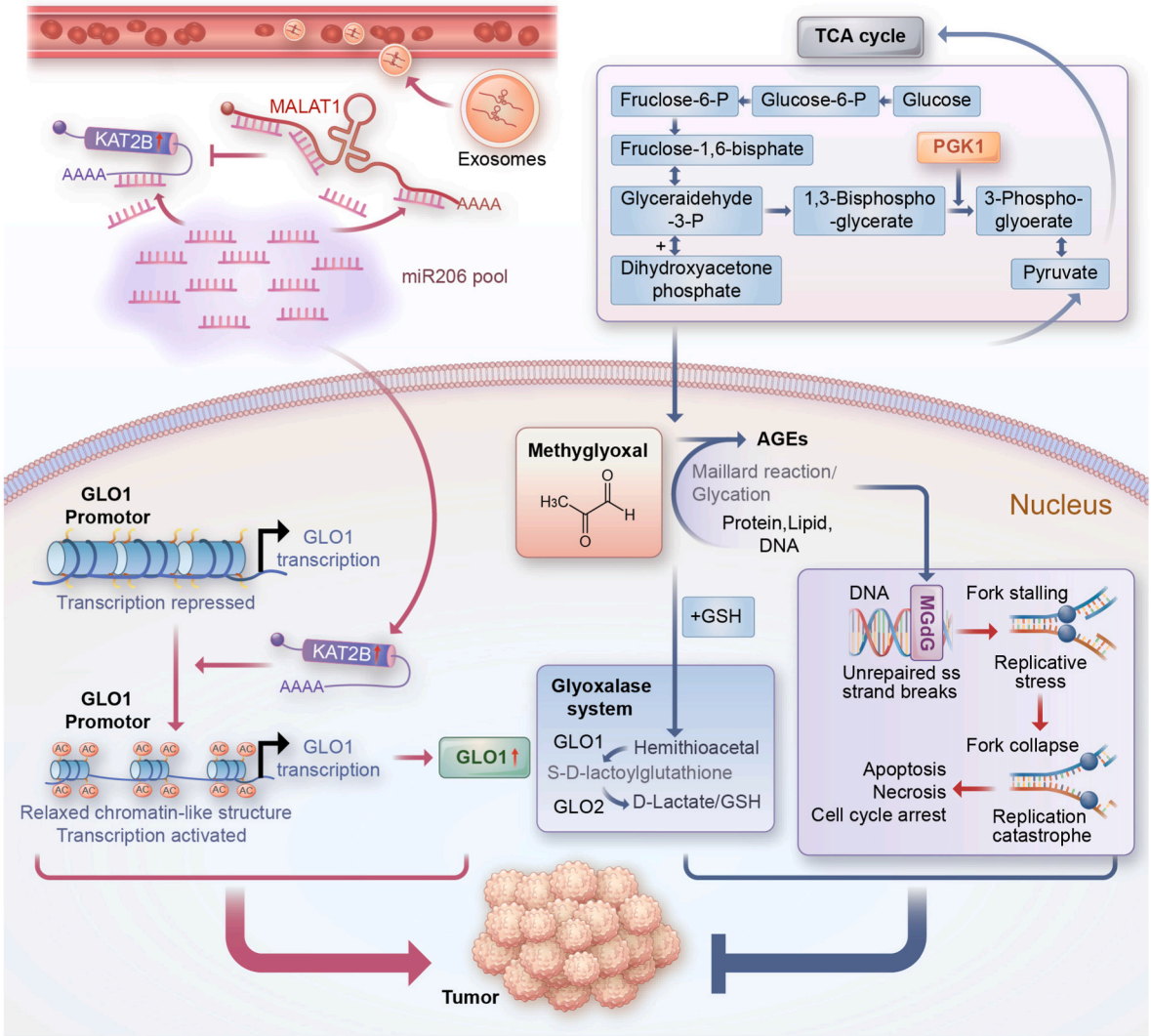

Fig. 8. Schematic diagram of the MALAT1-KAT2B-GLO1 regulatory network and its implications in the progression of ESCC
MALAT1 sponges miR-206 to alleviate its degradation of KAT2B mRNA, resulting in elevated KAT2B expression. KAT2B promotes GLO1 expression via epigenetic modification of the GLO1 promoter through histone acetylation. Overexpressed GLO1 detoxifies methylglyoxal, which is a by-product of tumor glycolysis and is cytotoxic to tumor cells. Finally, degradation of methylglyoxal by GLO1 enhanced tumor growth and metastasis. Moreover, MALAT1 is encapsulated by exosomes and released into circulation, resulting in malignant phenotypes that spread intercellularly, making liquid biopsy through exosomal MALAT1 possible.

Funding

This work was supported by the National Natural Science Foundation of China (No. 81702444), China Postdoctoral Science Foundation 2018M643884, and 2020T130128ZX, and Basic research project (Natural science funds) of Jiangsu Province [BK20160606].

CRediT authorship contribution statement

Liwen Hu: Project administration, Funding acquisition, Conceptualization. **Kai Xie:** Writing – original draft, Investigation, Formal analysis, Data curation. **Chao Zheng:** Methodology, Data curation. **Bingmei Qiu:** Resources, Formal analysis. **Zhisheng Jiang:** Resources, Investigation. **Chao Luo:** Methodology, Data curation. **Yifei Diao:** Validation, Formal analysis. **Jing Luo:** Writing – original draft, Validation. **Xinyue Yao:** Supervision, Investigation, Conceptualization. **Yi Shen:** Supervision, Conceptualization.

Declaration of competing interest

The authors declare that they have no known competing financial interests or personal relationships that could have appeared to influence the work reported in this paper.

Acknowledgments

None.

Abbreviations

ESCC	esophageal squamous cell carcinoma
lncRNA	long noncoding RNA
MALAT1	metastasis-associated lung adenocarcinoma transcript 1
GLO1	glyoxalase 1
KAT2B	lysine acetyltransferase 2 B
MGO	methylglyoxal
AGE	advanced glycation end products
CD63	CD63 molecule
ATM	ataxia telangiectasia mutated
BAX	BCL2 associated X
AKT	serine/threonine kinase 1
DMSO	dimethyl sulfoxide.

Appendix A. Supplementary data

Supplementary data to this article can be found online at https://doi.org/10.1016/j.ncrna.2024.01.003.

References

[1] C.C. Abnet, M. Arnold, W.Q. Wei, Epidemiology of esophageal squamous cell carcinoma, Gastroenterology 154 (2) (2018) 360–373.
[2] H. Sung, J. Ferlay, R.L. Siegel, M. Laversanne, I. Soerjomataram, A. Jemal, F. Bray, Global cancer statistics 2020: GLOBOCAN estimates of incidence and mortality worldwide for 36 cancers in 185 countries, CA Cancer J Clin 71 (3) (2021) 209–249.
[3] C. Xia, X. Dong, H. Li, M. Cao, D. Sun, S. He, F. Yang, X. Yan, S. Zhang, N. Li, et al., Cancer statistics in China and United States, 2022: profiles, trends, and determinants, Chin. Med. J. 135 (5) (2022) 584–590.
[4] X. Huang, X. Zhou, Q. Hu, B. Sun, M. Deng, X. Qi, M. Lu, Advances in esophageal cancer: a new perspective on pathogenesis associated with long non-coding RNAs, Cancer Lett. 413 (2018) 94–101.
[5] L. Hu, Y. Wu, D. Tan, H. Meng, K. Wang, Y. Bai, K. Yang, Up-regulation of long noncoding RNA MALAT1 contributes to proliferation and metastasis in esophageal squamous cell carcinoma, J. Exp. Clin. Cancer Res. 34 (2015) 7.
[6] X. Cao, R. Zhao, Q. Chen, Y. Zhao, B. Zhang, Y. Zhang, J. Yu, G. Han, W. Cao, J. Li, et al., MALAT1 might be a predictive marker of poor prognosis in patients who underwent radical resection of middle thoracic esophageal squamous cell carcinoma, Cancer Biomarkers 15 (6) (2015) 717–723.
[7] R.Q. Li, Y. Ren, W. Liu, W. Pan, F.J. Xu, M. Yang, MicroRNA-mediated silence of onco-lncRNA MALAT1 in different ESCC cells via ligand-functionalized hydroxyl-rich nanovectors, Nanoscale 9 (7) (2017) 2521–2530.
[8] X. Wang, M. Li, Z. Wang, S. Han, X. Tang, Y. Ge, L. Zhou, C. Zhou, Q. Yuan, M. Yang, Silencing of long noncoding RNA MALAT1 by miR-101 and miR-217 inhibits proliferation, migration, and invasion of esophageal squamous cell carcinoma cells, J. Biol. Chem. 290 (7) (2015) 3925–3935.
[9] M. Usami, K. Ando, A. Shibuya, R. Takasawa, H. Yokoyama, Crystal structures of human glyoxalase I and its complex with TLSC702 reveal inhibitor binding mode and substrate preference, FEBS Lett 596 (11) (2022) 1458–1467.
[10] J. Bellier, M.J. Nokin, E. Larde, P. Karoyan, O. Peulen, V. Castronovo, A. Bellahcene, Methylglyoxal, a potent inducer of AGEs, connects between diabetes and cancer, Diabetes Res. Clin. Pract. 148 (2019) 200–211.
[11] J. Morgenstern, M. Campos Campos, P. Nawroth, T. Fleming, The glyoxalase system-new insights into an ancient metabolism, Antioxidants 9 (10) (2020).
[12] N. Rabbani, M. Xue, M.O. Weickert, P.J. Thornalley, Multiple roles of glyoxalase 1-mediated suppression of methylglyoxal glycation in cancer biology-Involvement in tumour suppression, tumour growth, multidrug resistance and target for chemotherapy, Semin. Cancer Biol. 49 (2018) 83–93.
[13] F. Hosoda, Y. Arai, N. Okada, H. Shimizu, M. Miyamoto, N. Kitagawa, H. Katai, H. Taniguchi, K. Yanagihara, I. Imoto, et al., Integrated genomic and functional analyses reveal glyoxalase I as a novel metabolic oncogene in human gastric cancer, Oncogene 34 (9) (2015) 1196–1206.
[14] T. Yousefi, A.R.G. Pasha, G. Kamrani, A. Ebrahimzadeh, A. Zahedian, K. Hajian-Tilaki, M. Aghajani, D. Qujeq, Evaluation of Fructosamine 3-kinase and Glyoxalase 1 activity in normal and breast cancer tissues, Biomedicine 11 (3) (2021) 15–22.
[15] S. Yumnam, L. Subedi, S.Y. Kim, Glyoxalase system in the progression of skin aging and skin malignancies, Int. J. Mol. Sci. 22 (1) (2020).
[16] L. Rounds, R.B. Nagle, A. Muranyi, J. Jandova, S. Gill, E. Vela, G.T. Wondrak, Glyoxalase 1 expression as a novel diagnostic marker of high-grade prostatic intraepithelial neoplasia in prostate cancer, Cancers 13 (14) (2021).
[17] C. Antognelli, L. Marinucci, R. Frosini, L. Macchioni, V.N. Talesa, Metastatic prostate cancer cells secrete methylglyoxal-derived mg-H1 to reprogram human osteoblasts into a dedifferentiated, malignant-like phenotype: a possible novel player in prostate cancer bone metastases, Int. J. Mol. Sci. (19) (2021) 22.
[18] C. Antognelli, M. Mandarano, E. Prosperi, A. Sidoni, V.N. Talesa, Glyoxalase-1-Dependent methylglyoxal depletion sustains PD-L1 expression in metastatic prostate cancer cells: a novel mechanism in cancer immunosurveillance escape and a potential novel target to overcome PD-L1 blockade resistance, Cancers 13 (12) (2021).
[19] B.A. Al-Oudat, H.M. Jaradat, Q.A. Al-Balas, N.A. Al-Shar'i, A. Bryant-Friedrich, M. F. Bedi, Design, synthesis and biological evaluation of novel glyoxalase I inhibitors possessing diazenylbenzenesulfonamide moiety as potential anticancer agents, Bioorg. Med. Chem. 28 (16) (2020) 115608.
[20] S.A. Audat, Q.A. Al-Balas, B.A. Al-Oudat, M.J. Athamneh, A. Bryant-Friedrich, Design, synthesis and biological evaluation of 1,4-benzenesulfonamide derivatives as glyoxalase I inhibitors, Drug Des. Dev. Ther. 16 (2022) 873–885.
[21] C. Chen, H. Yu, F. Han, X. Lai, K. Ye, S. Lei, M. Mai, M. Lai, H. Zhang, Tumor-suppressive circRHOBTB3 is excreted out of cells via exosome to sustain colorectal cancer cell fitness, Mol. Cancer 21 (1) (2022) 46.
[22] S. Liu, W. Wang, Y. Ning, H. Zheng, Y. Zhan, H. Wang, Y. Yang, J. Luo, Q. Wen, H. Zang, et al., Exosome-mediated miR-7-5p delivery enhances the anticancer effect of Everolimus via blocking MNK/eIF4E axis in non-small cell lung cancer, Cell Death Dis. 13 (2) (2022) 129.
[23] P. Li, Z. Xu, T. Liu, Q. Liu, H. Zhou, S. Meng, Z. Feng, Y. Tang, C. Liu, J. Feng, et al., Circular RNA sequencing reveals serum exosome circular RNA panel for high-grade astrocytoma diagnosis, Clin. Chem. 68 (2) (2022) 332–343.
[24] L. Wang, J. Wu, N. Ye, F. Li, H. Zhan, S. Chen, J. Xu, Plasma-derived exosome MiR-19b acts as a diagnostic marker for pancreatic cancer, Front. Oncol. 11 (2021) 739111.
[25] S. Matsuoka, M. Huang, S.J. Elledge, Linkage of ATM to cell cycle regulation by the Chk2 protein kinase, Science 282 (5395) (1998) 1893–1897.
[26] V. Tripathi, Z. Shen, A. Chakraborty, S. Giri, S.M. Freier, X. Wu, Y. Zhang, M. Gorospe, S.G. Prasanth, A. Lal, et al., Long noncoding RNA MALAT1 controls cell cycle progression by regulating the expression of oncogenic transcription factor B-MYB, PLoS Genet. 9 (3) (2013) e1003368.
[27] Q.Y. Mao, S.Y. He, Q.Y. Hu, Y. Lu, Y.X. Niu, X.Y. Li, H.M. Zhang, L. Qin, Q. Su, Advanced glycation end products (AGEs) inhibit macrophage efferocytosis of apoptotic beta cells through binding to the receptor for AGEs, J. Immunol. 208 (5) (2022) 1204–1213.
[28] X.J. Chen, W.J. Wu, Q. Zhou, J.P. Jie, X. Chen, F. Wang, X.H. Gong, Advanced glycation end-products induce oxidative stress through the Sirt1/Nrf2 axis by interacting with the receptor of AGEs under diabetic conditions, J. Cell. Biochem. 120 (2) (2018) 2159–2170.
[29] A. Hutschenreuther, M. Bigl, N.Y. Hemdan, T. Debebe, F. Gaunitz, G. Birkenmeier, Modulation of GLO1 expression affects malignant properties of cells, Int. J. Mol. Sci. 17 (12) (2016).
[30] D. Tang, W. Xiao, W.T. Gu, Z.T. Zhang, S.H. Xu, Z.Q. Chen, Y.H. Xu, L.Y. Zhang, S. M. Wang, H. Nie, Pterostilbene prevents methylglyoxal-induced cytotoxicity in endothelial cells by regulating glyoxalase, oxidative stress and apoptosis, Food Chem. Toxicol. 153 (2021) 112244.
[31] A. Shafie, M. Xue, P.J. Thornalley, N. Rabbani, Copy number variation of glyoxalase I, Biochem. Soc. Trans. 42 (2) (2014) 500–503.
[32] Y.W. Liu, X.L. Liu, L. Kong, M.Y. Zhang, Y.J. Chen, X. Zhu, Y.C. Hao, Neuroprotection of quercetin on central neurons against chronic high glucose

through enhancement of Nrf2/ARE/glyoxalase-1 pathway mediated by phosphorylation regulation, Biomed. Pharmacother. 109 (2019) 2145–2154.
[33] R. Mastrocola, AGEs and neurodegeneration: the Nrf2/glyoxalase-1 interaction, Oncotarget 8 (4) (2017) 5645–5646.
[34] V. de Hemptinne, D. Rondas, M. Toepoel, K. Vancompernolle, Phosphorylation on Thr-106 and NO-modification of glyoxalase I suppress the TNF-induced transcriptional activity of NF-kappaB, Mol. Cell. Biochem. 325 (1–2) (2009) 169–178.
[35] M. Fournier, M. Orpinell, C. Grauffel, E. Scheer, J.M. Garnier, T. Ye, V. Chavant, M. Joint, F. Esashi, A. Dejaegere, et al., KAT2A/KAT2B-targeted acetylome reveals a role for PLK4 acetylation in preventing centrosome amplification, Nat. Commun. 7 (2016) 13227.
[36] T.K. Ghosh, J.J. Aparicio-Sanchez, S. Buxton, A. Ketley, T. Mohamed, C.S. Rutland, S. Loughna, J.D. Brook, Acetylation of TBX5 by KAT2B and KAT2A regulates heart and limb development, J. Mol. Cell. Cardiol. 114 (2018) 185–198.
[37] W.S. Lian, J.Y. Ko, Y.S. Chen, H.J. Ke, C.K. Hsieh, C.W. Kuo, S.Y. Wang, B. W. Huang, J.G. Tseng, F.S. Wang, MicroRNA-29a represses osteoclast formation and protects against osteoporosis by regulating PCAF-mediated RANKL and CXCL12, Cell Death Dis. 10 (10) (2019) 705.
[38] R. Chaudhari, S. Nasra, N. Meghani, A. Kumar, MiR-206 conjugated gold nanoparticle based targeted therapy in breast cancer cells, Sci. Rep. 12 (1) (2022) 4713.
[39] R. Yang, D. Wang, S. Han, Y. Gu, Z. Li, L. Deng, A. Yin, Y. Gao, X. Li, Y. Yu, et al., MiR-206 suppresses the deterioration of intrahepatic cholangiocarcinoma and promotes sensitivity to chemotherapy by inhibiting interactions with stromal CAFs, Int. J. Biol. Sci. 18 (1) (2022) 43–64.
[40] C. Liu, J. Li, W. Wang, X. Zhong, F. Xu, J. Lu, miR-206 inhibits liver cancer stem cell expansion by regulating EGFR expression, Cell Cycle 19 (10) (2020) 1077–1088.
[41] Y. Liu, Y. Song, X. Chen, J. Fan, W. Zheng, C. Cao, miR-206 inhibits laryngeal carcinoma cell multiplication, migration, and invasion, J Healthc Eng 2021 (2021) 5614861.
[42] Y. Tang, G. Xiao, Y. Chen, Y. Deng, LncRNA MALAT1 promotes migration and invasion of non-small-cell lung cancer by targeting miR-206 and activating Akt/mTOR signaling, Anti Cancer Drugs 29 (8) (2018) 725–735.
[43] H. Jing, C. Wang, L. Zhao, J. Cheng, P. Qin, H. Lin, Propofol protects cardiomyocytes from hypoxia/reoxygenation injury via regulating MALAT1/miR-206/ATG3 axis, J. Biochem. Mol. Toxicol. 35 (10) (2021) e22880.
[44] L. Min, T. Zhu, B. Lv, T. An, Q. Zhang, Y. Shang, Z. Yu, L. Zheng, Q. Wang, Exosomal LncRNA RP5-977B1 as a novel minimally invasive biomarker for diagnosis and prognosis in non-small cell lung cancer, Int. J. Clin. Oncol. 27 (6) (2022) 1013–1024.
[45] S. Nafar, N. Nouri, M. Alipour, J. Fallahi, F. Zare, S.M.B. Tabei, Exosome as a target for cancer treatment, J. Invest. Med. 70 (5) (2022) 1212–1218.